PCCP

Accepted Manuscript

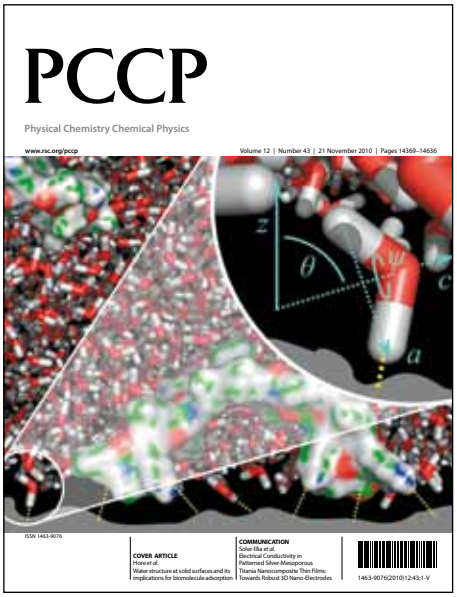

This is an *Accepted Manuscript*, which has been through the RSC Publishing peer review process and has been accepted for publication.

Accepted Manuscripts are published online shortly after acceptance, which is prior to technical editing, formatting and proof reading. This free service from RSC Publishing allows authors to make their results available to the community, in citable form, before publication of the edited article. This *Accepted Manuscript* will be replaced by the edited and formatted *Advance Article* as soon as this is available.

To cite this manuscript please use its permanent Digital Object Identifier (DOI®), which is identical for all formats of publication.

More information about *Accepted Manuscripts* can be found in the **Information for Authors**.

Please note that technical editing may introduce minor changes to the text and/or graphics contained in the manuscript submitted by the author(s) which may alter content, and that the standard **Terms & Conditions** and the **ethical guidelines** that apply to the journal are still applicable. In no event shall the RSC be held responsible for any errors or omissions in these *Accepted Manuscript* manuscripts or any consequences arising from the use of any information contained in them.

Ligand-field DFT versus Time-Dependent DFT on transition-metal cyclononane complexes, which one works better?

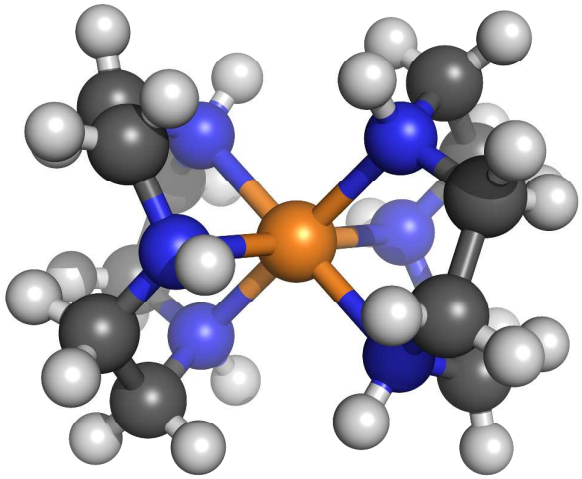

PCCP

Dynamic Article Links ►

Cite this: DOI: 10.1039/c0xx00000x

www.rsc.org/xxxxxx

PAPER

View Article Online

Computational study of the spin-state energies and UV-Vis spectra of bis(1,4,7-triazacyclononane) complexes of some first-row transition metal cations†

Matija Zlatar,[a] Maja Gruden-Pavlović,[b,*] Mireia Güell[c] and Marcel Swart[c,d,*]

Received (in XXX, XXX) Xth XXXXXXXXX 200X, Accepted Xth XXXXXXXXX 200X

DOI: 10.1039/b000000x

We report here computed spin-state energies and UV-Vis spectra for several transition metal complexes with a triazacyclononane ligand. Our results show that the spin ground-state is correctly obtained with either OPBE or SSB-D, except for the high-spin ground-state of the Co(II) complex that was properly described only by SSB-D. The UV-Vis spectra from TD-DFT reproduce in general rather well the experimental spectra, but in case of the Cr(III) and Co(II) complexes it clearly failed. Better results for the UV-Vis spectra have been obtained by using Ligand Field DFT.

Introduction

In organometallic and bioinorganic chemistry many reactions involve several electronic states, and reactivity often crucially depends on the preferred spin state of reactants, products, intermediates and transition states.[1-3] Orbital occupation patterns play an important role in enzymatic reactions (e.g. cytochrome P450cam),[4] in metal-oxo complexes, in spin-crossover compounds,[5-7] and there exists even spin-state catalysis where different reactions take place for different spin states.[8] Molecular switching due to thermally induced spin-crossover in transition metal (TM) compounds has raised much interest, in part because of the potential applications in technology and biomedicine.[9] The switch from low to high spin is usually accompanied by a change in metal–ligand bond lengths, changes of spectroscopic observables, reactivity, magnetic and other properties. One of the interesting aspects in this respect is the investigation of complexes containing a metal center with an electronic configuration that in a different ligand field exhibits the Jahn-Teller (JT) distortions,[10, 11] depending on the spin state. Therefore, it is necessary to have an accurate theoretical model to explain and predict spin state preferences, and computational studies have become invaluable in this area of research.

From a broad palette of electronic structure methods, Density Functional Theory (DFT)[12-14] emerged into the mainstream of quantum chemical methods, mainly because it gives a good compromise between accuracy of the results and computational efficiency. Even though DFT methods are in general very accurate for structures and energies, the reliable prediction of the correct ground state from a number of close lying states of different spin is a challenging problem. This is in particular so when transition metal systems are considered, and the predicted ground state will strongly depend on the choice of the exchange−correlation (XC) functional and the basis set used.[3, 15-17] Different XC approximations have often a bias towards either high-spin or low-spin states.[18] Our validation studies of DFT functionals[15, 19] have shown the excellent performance of the OPBE functional,[20-22] for capturing spin state diversity in iron complexes[19, 23] which is corroborated by good results in other studies.[18, 24-34] Therefore, one of the aims of the present work was to validate the performance of the (pure DFT) OPBE functional, but also the recently developed SSB-D functional.[35, 36] Here, we have performed a systematic investigation of the spin-state splittings and UV-VIS spectra for complexes of the *bis*(1,4,7-triazacyclononane) (TACN) with several first-row transition metal ions (see Figure 1).

Figure 1. $M(TACN)_2^{2+/3+}$ complexes (M=Cr, Mn, Fe, Co, Ni)

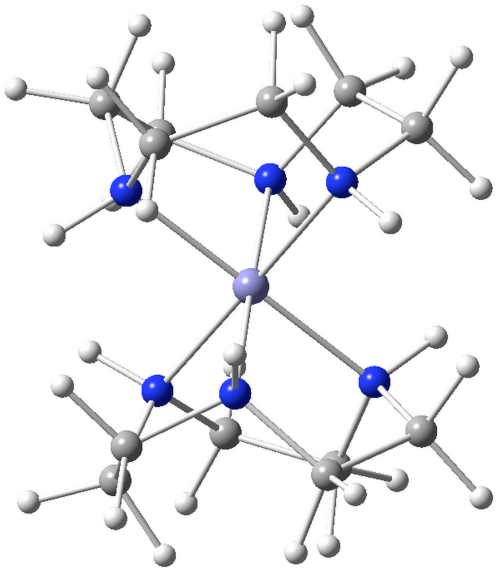

These systems have been well studied,[37] and were chosen due to their interesting properties, and the extensive experimental data available in the bibliography, with which we can compare our computed data. The possibility to correctly predict the spin ground-state of transition-metal complexes would enable the application of the methods to even more demanding situations. One of these situations is for instance spin flips that occur frequently in catalytic cycles of transition-metal enzymes and/or biomimetic analogues of these.

Since its original preparation in 1972,[38] and the subsequent synthesis of a series of transition-metal complexes,[39] it has been recognized that the cyclic amine TACN is a strong tridentate chelating ligand.[40] It is able to form very stable, distorted, octahedral *bis* complexes with many divalent and trivalent metal cations of the first transition metal series.[37] To date, first row transition metal octahedral complexes containing two such ligands of chromium(III),[41] manganese(II),[41, 42] iron(II),[41, 43] iron(III),[41, 43] cobalt(II),[41, 44] cobalt(III),[38] nickel(II),[39, 45] nickel(III),[41, 46] copper(II),[39] and zinc(II),[47] have been isolated and characterized. Their redox potentials were readily measured by cyclic voltammetry,[41] and the electron-transfer self-exchange rate constants of the $M(TACN)_2^{+3/+2}$ couples were determined and successfully interpreted.[37, 48, 49] Furthermore, it has been recognized that TACN and its N-alkylated derivatives are excellent ligands in supporting both mono- and bi-metallic complexes containing labile coordination sites. Hence, many of TACN complexes are found to be both structural and functional models of various metallo-enzymes, such as hemerythrin, phosphate esterases and copper-monooxygenases.

Two tridentately coordinated TACN ligands form a trigonally distorted octahedron, belonging to the D_3 point group, Figure 1. Since the TACN ligand is a pure sigma donor, *d* electrons on the metal ion can couple up in different ways to give either a high or low (or an intermediate) overall spin. More complications may arise if, due to the electronic configuration, static or dynamic JT distortion of the MN_6 core is present. Experimental studies of the cations $[Ni(TACN)_2]^{3+}$,[46] and $[Cu(TACN)_2]^{2+}$,[50, 51] showed evidence for the JT coupling. Therefore, the JT parameters, which describe the Adiabatic Potential Energy Surface of the JT active species, were determined by means of the Multi-Determinantal DFT (MD-DFT)[52, 53] and Intrinsic Distortion Path (IDP)[53-55] methods. To the best of our knowledge, there were no attempts so far in the literature to describe spin state splitting taking into account the vibronic couplings in these systems in detail, with the aid of theoretical/computational methods.

Computational Details

The calculations using the unrestricted formalism have been performed with the Amsterdam Density Functional (ADF) program package, version 2012.01.[56-58] MOs were expanded in an uncontracted set of Slate type orbitals (STOs) of triple-zeta quality containing diffuse functions and two sets of polarization functions (TZ2P) with small frozen core.[59] Energies and gradients were calculated using the local density approximation (LDA), with Slater exchange and VWN correlation.[60] In addition, gradient-corrections (GGA) for exchange (OPTX)[21] and correlation (PBE)[22] has been included self-consistently, i.e. the OPBE functional,[20] as well as the dispersion corrected functional by Swart-Solà-Bickelhaupt (SSB-D).[35, 36] Geometries were optimized constraining the symmetry to either the D_3 or C_2 point groups with the QUILD program,[61] provided in the ADF program package, using adapted delocalized coordinates,[62] until the maximum gradient component was less than $1.0 \cdot 10^{-4}$ atomic units. For the geometry optimization with the SSB-D functional, the developer version of ADF was used. In order to check the possible influence of an environment, mainly of water as a typical solvent used in experimental studies of these types of compounds, single point OPBE calculations with a dielectric continuum model (COSMO)[63-65] as implemented in ADF,[66, 67] were performed on the OPBE geometries.

In order to tackle the degenerate states, Multi-Determinantal DFT (MD-DFT),[52, 53] proven to be accurate for determination of the JT parameters,[52, 55, 68-70] have been performed. This procedure consists of the following steps: (i) an average-of-configuration (AOC) calculation in the D_3 point group, yielding the geometry of the high symmetry species; (ii) a single-point calculation imposing high symmetry on the nuclear geometry and low symmetry on the electron density, which is achieved by introducing an adequate occupation scheme of the MOs, and using a *symrot* sub-block in the QUILD program[61]; (iii) geometry optimization constraining the structure to the C_2 point group, with a specific orbital occupancy. The JT stabilization energy, E_{JT}, is the difference between the energies obtained in steps (ii) and (iii) with the same electron distribution; the warping barrier ($2B$) is the difference in energy between the two distorted structures with different electron distributions, step (iii).

The multimode JT problem was analyzed using the Intrinsic Distortion Path (IDP) model,[53-55] in which the JT distortion is expressed as a linear combination of all totally symmetric normal modes in the distorted, lower symmetry structure. The model allows quantification of the importance of all the involved normal modes along a steepest descent path from the symmetric (D_3) to the lower-symmetry minimum energy structure (C_2). Details about this approach can be found elsewhere.[55]

Excitation energies were calculated with the Time-Dependent DFT (TD-DFT) formalism,[71] as implemented in ADF,[72] with the OPBE functional and COSMO solvation model on the geometries optimized with LDA and OPBE.

The multiplet structure of the investigated complexes has also been calculated using LF-DFT, a DFT-based Ligand Field Theory,[73, 74] exhaustively described elsewhere,[73-79] on the LDA and OPBE optimized geometries using the OPBE functional and the COSMO solvation model. Briefly, this procedure consists of the following steps: i) an AOC spin-restricted calculation with *n* electrons distributed evenly over the five Kohn-Sham (KS) molecular orbitals dominated by metal *d* orbitals; ii) starting from the KS AOC orbitals, the energies of all Slater Determinants (SD) originated from the d^n shell are calculated in a spin-unrestricted way (120 for d^3 and d^7, 210 for d^6 and 252 for d^5 systems); iii) the SD energies and components of the corresponding AOC KS eigenvectors are used to determine the parameters of inter-electronic repulsion (Racah parameters *B* and *C*), and one-electron 5x5 LF matrix in a least-square sense; iv) these parameters are subsequently used as input for a conventional LF program allowing calculating all the multiplets using a configuration interaction (CI) of the full LF-manifold.

Results and Discussion

As already mentioned in the Introduction, herein we report the spin state splittings for a series of $[M(TACN)_2]^{2+/3+}$ complexes, where $M^{2+/3+}$ is: Cr^{3+}, Mn^{2+}, Fe^{3+}, Fe^{2+}, Co^{3+}, Co^{2+} and Ni^{3+}, respectively. Differently to the work of Lord *et al.*,[48] we examined the highest possible symmetry for the *bis*-TACN coordination, D_3, in pseudo-octahedral environment. In the D_3 point group, the degeneracy of the t_{2g} orbital set as present in the O_h point group is partially removed. Hence the frontier orbitals, dominated by *d*-orbitals of the metal cation, are of type: *e*, *a*, and *e*. In the case of electronic states that arise from the splitting of the triple degenerate states in O_h point group, e.g. $^2T_{1g}$ in Cr^{3+}, $^5T_{2g}$ in Co^{3+} and Fe^{2+} or $^4T_{1g}$ in Co^{2+} and Ni^{3+}, the relative order of *A* and *E* states in D_3 symmetry was surveyed, in order to be sure that the lowest energy one for each spin state is ascertained. Particular attention is paid to the deviation from D_3 to C_2 symmetry due to the JT effect in the case of degenerate electronic states. The results obtained with different XC functionals are summarized in Table 1, relative to the ground electronic state for that particular level of theory. They are overall consistent and in agreement with experimental findings.

Density functional theory with the OPBE functional has been used, due to the proven accuracy for this type of problems.[23] In addition, one of the aims of this work is to test the performance of the SSB-D functional, designed specifically to treat the issue of the spin-state splitting in addition to a proper treatment of S_N2 barriers.[35, 36] Although it is well known that LDA has a very poor performance considering relative spin-state energies of TM complexes (see e.g. ref. [80]), it is found to be accurate for geometries and vibrations of the coordination compounds,[70, 81] for the description of the adiabatic potential energy surfaces of a particular spin state, and for the determination of the vibronic coupling parameters, e.g. E_{JT}, in a variety of chemical species.[68] Importantly, due to its simplicity, LDA is fast, and can open a door for the everyday study of much larger systems than for example of those studied here. While in general there is an

Table 1 Spin state energies (kcal·mol^{-1}) relative to the ground electronic state for particular level of theory, for $[M(TACN)_2]^{2+/3+}$ complex ions, $M^{2+/3+}$ is: Cr^{3+}, Mn^{2+}, Fe^{3+}, Fe^{2+}, Co^{3+}, Co^{2+}, Ni^{3+}.

					Level of Theory					
M^{n+}	d^n	Symm.	Spin state[a]	State	LDA[b]	OPBE//LDA[c]	OPBE[b]	SSB-D[b]	OPBE/COSMO[d]	exp.[e]
Cr^{3+}	d^3	D_3	HS	$^4A_2$	0	0	0	0	0	HS
			LS	$^2A_2$	37.5	49.9	50.5	47.1	49.5	
Mn^{2+}	d^5	D_3	HS	$^6A_1$	9.53	0	0	0	0	HS
			IS	^4E	11.69	39.23	37.84	35.18	35.48	
			LS	^2E	0.25	37.52	38.02	32.89	33.59	
		C_2	IS	^4B	6.40	32.67	32.43	29.84	30.48	
			LS	^2A	0	37.07	37.80	32.30	33.48	
Fe^{3+}	d^5	D_3	HS	$^6A_1$	41.66	6.15	6.57	6.64	13.07	LS
			IS	^4E	32.91	15.17	13.42	13.73	17.30	
			LS	^2E	0.19	0.71	0.20	0.28	0	
		C_2	IS	^4B	28.61	10.61	9.84	10.71	13.93	
			LS	^2A	0	0	0	0	0	
Fe^{2+}	d^6	D_3	HS	$^5A_1$	38.82	1.64	2.02	1.28	3.34	LS
				^5E	39.88	0	0	0.09	1.38	
			IS	^3E	34.33	17.36	18.20	16.47	18.03	
			LS	$^1A_1$	0	1.00	2.43	1.73	0	
		C_2	HS	^5B	39.93	0	0	0	1.65	
			IS	^3B	30.29	13.77	13.93	14.53	13.43	
Co^{3+}	d^6	D_3	HS	$^5A_1$	74.22	45.72	45.05	43.48	51.99	LS
			IS	^3E	51.04	39.65	32.63	30.20	35.89	
			LS	$^1A_1$	0	0	0	0	0	
		C_2	IS	^3B	45.19	29.93	29.02	28.33	32.25	
Co^{2+}	d^7	D_3	HS	$^4A_1$	23.65	3.58	3.13	2.54	4.85	HS
				^4E	20.92	1.32	0.42	0.02	2.24	
			LS	^2E	5.66	6.02	4.57	7.3	5.79	
		C_2	HS	^4B	20.85	0.88	0.34	0	2.33	
			LS	^2A	0	0	0	2.17	0	
Ni^{3+}	d^7	D_3	HS	$^4A_1$	49.70	34.37	33.99	32.79	37.80	LS
				^4E	45.00	30.39	29.93	30.01	34.14	
			LS	^2E	4.29	4.25	4.1	3.46	3.83	
		C_2	HS	^4B	42.22	28.32	27.77	27.62	31.66	
			LS	^2A	0	0	0	0	0	

[a]HS – high-spin; LS – low-spin; IS – intermediate-spin.

[b]Geometry optimizations.

[c]Single point OPBE calculations on LDA geometries.

[d]Single point OPBE calculations with COSMO (water as solvent) on OPBE geometries.

[e]Exp. determined spin-state: Cr^{3+}, Mn^{2+}, Fe^{3+} ref.[41] ; Fe^{2+} ref.[41, 84] ; Co^{3+} ref.[38] ; Co^{2+} ref.[41, 44] ; Ni^{3+} ref.[41,46]

excellent agreement between LDA geometries and observed X-ray data (Table S1 in Supplementary information), as expected, LDA gives good spin-state energies only in "simple" cases like Cr^{3+}, Co^{3+} or Ni^{3+}. Completely wrong ground states and spin-state energies have been found with LDA for the Mn^{2+} and Co^{2+} complexes, as well as too large energy differences between the high-spin and low-spin states of Fe^{2+}/Fe^{3+} (see Table 1). However, if single point (fully self-consistent) OPBE DFT calculations were performed on LDA geometries, the results concur with OPBE or SSB-D optimizations (Table 1). Therefore, although LDA cannot be trusted for the spin-state energies, the geometries it provides are good.

A. Spin-state energies of TM complexes

For the $[Cr(TACN)_2]^{3+}$ cation, as expected, a quartet state is found to be the ground state (see Table 1). The high lying doublet state was found to show non-negligible spin contamination, i.e. an expectation value of S^2 of 1.76 (a pure spin doublet has an S^2 value of 0.75). The spin projection technique was used,[82] both for the energy and the gradients,[61, 83] to obtain the results for the pure spin doublet. Similarly, irrespectively of the functional used, the low-spin $^1A_1$ state for $[Co(TACN)_2]^{3+}$ is the most stable one. These two metal cations do not have reasonable alternative spin states, as expected.

Our calculations for $[Mn(TACN)_2]^{2+}$ clearly indicate $^6A_1$ as the ground-state. However, both low-spin and intermediate-spin are subject to JT distortion, where the reduction in symmetry leads to a complex with C_2 symmetry. The results, shown in Table 1, reveal that the additional JT stabilization is only minor compared to the initial destabilization with respect to the ground-state, i.e. after JT distortion, the symmetric high-spin ground-state remains ca. 30 kcal·mol^{-1} lower in energy. This is not surprising, because the unpaired electron in the low-spin configuration is located in the non-bonding degenerate e orbitals, originating from the t_{2g} orbitals in O_h point group, hence this system is similar to the $T\otimes(t+e)$ JT distortion, which is well known to be small.[11] On the other hand, the symmetry lowering of the strongly anti-bonding ^4E state, corresponding to the intermediate-spin, is a typical example of the $E\otimes e$ JT problem. Even though it is larger than in the previous case, the stabilization energy is still insufficient to surpass the large original spin-splitting.

In spite of the fact that both Mn^{2+} and Fe^{3+} have a d^5 electron configuration, different ground-states for $[Mn(TACN)_2]^{2+}$ and $[Fe(TACN)_2]^{3+}$ are predicted in the D_3 environment, i.e. a $^6A_1$ for the former and ^2E for the latter, which is in agreement with the experimental findings.[41] A trigonal type of distortion occurs in the low-spin $[Fe(TACN)_2]^{3+}$ complex cation, where the distorted C_2 ^2A structure is found to be the ground-state, with a stabilization energy of only 0.2-0.8 kcal·mol^{-1} with respect to the corresponding ^2E state.

Our DFT calculations for $[Fe(TACN)_2]^{2+}$ disclosed that the spin-state energies are more susceptible to the choice of XC functional. Moreover, vibronic coupling effects differ in the high-spin and intermediate-spin states, but do not have an effect on the total energy order of the states. If we exclude results obtained with the simplest functional (LDA), the energy difference between the high-spin and low-spin states is of the order of 1-2 kcal·mol^{-1}, which reproduces nicely the well-established spin-flexibility of Fe(II) compounds and the related spin-crossover behavior of $[Fe(TACN)_2]^{2+}$.[84] Both OPBE and SSB-D gas-phase optimizations revealed a ^5B state within C_2 symmetry, derived from the high-spin ^5E state as the most stable one, although the JT stabilization is almost negligible. Intermediate-spin in the high symmetry point group is the subject of the $E\otimes e$ JT problem, where the descent in symmetry gives energy stabilization of about 4 kcal·mol^{-1}, not enough to overcome the initial spin-state splitting. The experimentally found low-spin ground state[84] is obtained when solvation effects are included, suggesting that small perturbation of the environment can cause different preferential for spin-states.

In the D_3 nuclear arrangement of $[Co(TACN)_2]^{2+}$ the ground state can be either ^2E (low-spin configuration) or ^4E (high-spin configuration). The high-spin state is found to be more stable (see Table 1), corroborating with the experimental observations.[41] Very small trigonal distortion of the high-spin configuration and larger tetragonal distortion in the low-spin state are observed, with a descent in symmetry to the C_2. The SSB-D functional captures the experimentally observed high-spin state, while with other functionals the ^2A state is predicted to be the ground state; the ^2A state is an electronic state arising from the low-spin ^2E state in D_3 point group.

The Ni^{3+} ion is isoelectronic with and has the same order of orbitals as the Co^{2+} ion. We observed the ^2A state in C_2 symmetry as the ground state, corresponding to the distortion from the low-spin ^2E state, irrespective of the level of theory. While $[Co(TACN)_2]^{2+}$ can be considered as spin-crossover compound, in $[Ni(TACN)_2]^{3+}$ the difference in energy between the low-spin and high-spin states is much higher.

B. Jahn-Teller distortions

All the complexes under investigation here which are prone to JT distortion have an E electronic ground state in the high symmetry nuclear configuration, i.e. the D_3 point group. This nuclear configuration is not a stationary point on the potential energy surface, at which there exists coupling between the E electronic state with the non-totally-symmetric, e, vibrations, leading to distorted C_2 structures. The theory behind this vibronic coupling is well documented in the book by Bersuker.[11]

Generally speaking, there are two types of distortions of the MN_6 octahedral core, depending on the electronic configuration and occupation of the d levels. In D_3 symmetry there are two sets of e orbitals: non-bonding (originating from t_{2g} in O_h), and higher-lying anti-bonding type (originating from e_g in O_h). If the non-bonding e orbitals are partially filled, the distortion is very small and can be nominally treated as coupling between the T_{2g} state with t_{1g} vibrations in the O_h point group. When anti-bonding e orbitals are unequally occupied, a distortion will result in an elongated/compressed octahedron. Both types of deformation remove the degeneracy leading to two distorted structures, corresponding to the minimum and transition state, respectively, on the Adiabatic Potential Energy Surface. Results of MD-DFT calculations performed to analyze the JT effect in complexes prone to the JT distortion are depicted in Table 2 and Table 3. In order to make a comparison with systems that exhibit a strong JT coupling, but no spin-state preferences, the results for $[Cu(TACN)_2]^{2+}$ are also presented (Table 3); this latter system is very well characterized experimentally. The values of the JT parameters are fully in agreement with experimentally evaluated

Table 2 Results of the MD-DFT calculations performed to analyze the JT effect in degenerate states of $[M(TACN)_2]^{2+/3+}$ complex ions; $M^{2+/3+}$ is: Mn^{2+}, Fe^{3+} and Fe^{2+}; energies and the JT parameters (E_{JT} and $2B$) are given in kcal·mol^{-1}.

Spin state[a]		LDA[b]	OPBE//LDA[c]	OPBE[b]	SSB-D[b]	OPBE/COSMO[d]
Mn^{2+}						
IS	^4E(AOC)	-6494.6	--	-6059.7	-6269.7	--
	$^4E(A)$	-6494.1	-6055.4	-6062.6	-6272.0	-6213.1
	$^4E(B)$	-6496.1	-6056.3	-6063.7	-6273.1	-6214.3
	^4A	-6498.7	-6059.9	-6066.2	-6276.2	-6217.1
	^4B	-6501.3	-6062.8	-6069.1	-6278.5	-6219.3
	E_{JT}(A)	4.64	4.53	3.65	4.15	4.02
	E_{JT}(B)	5.29	6.56	5.41	5.34	5.00
	$2B$	2.65	2.9	2.86	2.29	2.15
LS	^2E(AOC)	-6517.0	--	-6060.2	-6271.5	--
	$^2E(A)$	-6517.0	-6058.0	-6063.5	-6275.4	-6216.1
	$^2E(B)$	-6516.9	-6057.8	-6063.3	-6275.3	-6215.9
	^2A	-6517.3	-6058.4	-6063.7	-6276.0	-6216.3
	^2B	-6517.2	-6058.2	-6063.5	-6275.9	-6216.1
	E_{JT}(A)	0.25		0.22	0.59	0.11
	E_{JT}(B)	0.27		0.19	0.58	0.14
	$2B$	0.05	0.24	0.22	0.13	0.16
Fe^{3+}						
IS	^4E(AOC)	-6186.9	--		-5959.7	--
	$^4E(A)$	-6187.6	-5747.5	-5754.0	-5961.9	-6092.7
	$^4E(B)$	-6188.9	-5748.5	-5755.3	-5963.2	-6094.0
	^4A	-6190.9	-5750.9	-5756.9	-5964.4	-6095.4
	^4B	-6193.2	-5753.1	-5758.9	-5966.2	-6097.4
	E_{JT}(A)	3.39	3.48	2.9	2.52	2.76
	E_{JT}(B)	4.3	4.56	3.58	3.02	3.37
	$2B$	2.25	2.14	1.98	1.79	1.96
LS	^2E(AOC)	-6221.9	--		-5972.4	--
	$^2E(A)$	-6221.6	-5763.0	-5768.5	-5976.7	-6111.3
	$^2E(B)$	-6221.5	-5763.3	-5768.3	-5976.5	-6111.0
	^{2}A	-6221.8	-5763.7	-5768.7	-5976.9	-6111.3
	^{2}B	-6221.8	-5763.4	-5768.4	-5976.7	-6111.0
	E_{JT}(A)	0.19	0.71	0.20	0.28	0
	E_{JT}(B)	0.2	0.14	0.15	0.25	0
	$2B$	0.09	0.3	0.32	0.21	0.32
Fe^{2+}						
IS	^3E(AOC)	-6482.1	--	-6038.1	-6250.9	--
	$^3E(A)$	-6485.2	-6036.2	-6042.6	-6256.5	-6193.8
	$^3E(B)$	-6489.4	-6039.9	-6045.6	-6259.5	-6196.8
	^3A	-6490.7	-6041.9	-6048.3	-6260.6	-6199.6
	^3B	-6493.4	-6043.5	-6049.9	-6262.6	-6201.4
	E_{JT}(A)	5.51	5.72	5.70	4.13	5.75
	E_{JT}(B)	4.04	3.59	4.27	3.07	4.60
	$2B$	2.65	1.62	1.57	1.97	1.79
	R_{JT}					
HS	^5E(AOC)	-6484.0	--	-6059.9	-6271.9	--
	$^5E(A)$	-6483.6	-6056.6	-6063.7	-6275.9	-6213.3
	$^5E(B)$	-6483.7	-6057.4	-6063.9	-6277.0	-6213.4
	^5A	-6483.6	-6057.0	-6063.8	-6276.9	-6213.1
	^5B	-6483.8	-6057.3	-6063.9	-6277.1	-6213.1
	E_{JT}(A)	0.09	0.37	0.01	1.00	-0.23
	E_{JT}(B)	0.05	-0.05	0.002	0.09	-0.27
	$2B$	0.11	0.03	0.10	0.2	0.07

[a]HS – high-spin; LS – low-spin; IS – intermediate-spin.

[b]Geometry optimizations.

[c]Single point OPBE calculations on LDA geometries.

[d]Single point OPBE calculations with COSMO (water as solvent) on OPBE geometries.

Table 3. Results of the MD-DFT calculations performed to analyze the JT effect in degenerate states of $[M(TACN)_2]^{2+/3+}$ complex ions; $M^{2+/3+}$ is: Co^{3+}, Co^{2+}, Ni^{3+} and Cu^{2+}; energies and the JT parameters (E_{JT} and $2B$) are given in kcal·mol^{-1}.

Spin state[a]		LDA[b]	OPBE//LDA[c]	OPBE[b]	SSB-D[b]	OPBE/COSMO[d]
Co^{3+}						
IS	^3E(AOC)	-6165.8	--	-5720.5	-5928.7	--
	$^3E(A)$	-6165.3	-5710.2	-5722.9	-5931.9	-6063.3
	$^3E(B)$	-6168.6	-5713.2	-5725.1	-5934.4	-6065.4
	^3A	-6171.5	-5721.1	-5726.9	-5934.5	-6066.8
	^3B	-6174.4	-5722.9	-5728.7	-5936.3	-6069.0
	E_{JT}(A)	6.2	10.87	4.01	2.58	3.47
	E_{JT}(B)	5.85	9.72	3.61	1.87	3.64
	$2B$	2.96	1.80	1.79	1.80	2.24
Co^{2+}						
LS	^2E(AOC)	-6486.0	--	-6030.7	-6243.3	--
	$^2E(A)$	-6483.9	-6023.3	-6029.5	-6243.1	-6182.0
	$^2E(B)$	-6484.0	-6023.6	-6029.7	-6243.3	-6182.1
	^2A	-6489.5	-6029.4	-6035.6	-6248.2	-6187.8
	^2B	-6488.2	-6027.9	-6034.1	-6247.2	-6186.2
	E_{JT}(A)	5.66	6.02	4.57	5.13	6.28
	E_{JT}(B)	4.2	4.35	4.41	3.95	4.16
	$2B$	1.33	1.45	1.45	0.96	2.07
HS	^4E(AOC)	-6468.7	--	-6030.9	-6244.7	--
	$^4E(A)$	-6468.5	-6027.8	-6034.9	-6250.2	-6185.4
	$^4E(B)$	-6468.6	-6028.0	-6035.1	-6250.3	-6185.6
	^4A	-6468.6	-6028.3	-6035.0	-6250.2	-6185.3
	^4B	-6468.7	-6028.5	-6035.2	-6250.4	-6185.5
	E_{JT}(A)	0.11	0.47	0.08	0.005	-0.03
	E_{JT}(B)	0.07	0.44	0.08	0.02	-0.09
	$2B$	0.07	0.22	0.20	0.17	0.17
Ni^{3+}						
LS	^2E(AOC)	-6115.2	--	-5651.5	-5865.7	--
	$^2E(A)$	-6113.4	-5644.3	-5650.3	-5865.0	-5991.3
	$^2E(B)$	-6113.5	-5644.5	-5650.4	-5865.2	-5991.3
	^2A	-6117.7	-5648.6	-5654.4	-5868.5	-5995.1
	^2B	-6117.1	-5648.1	-5653.9	-5868.2	-5994.9
	E_{JT}(A)	4.29	4.25	4.1	3.46	3.83
	E_{JT}(B)	3.62	3.58	3.48	3.06	3.56
	$2B$	0.55	0.51	0.45	0.23	0.27
HS	^4E(AOC)	-6073.0	--	-5623.0	-5836.8	--
	$^4E(A)$	-6072.7	-5618.2	-5624.4	-5839.0	-5961.0
	$^4E(B)$	-6072.7	-5618.2	-5624.4	-5839.0	-5961.0
	^4A	-6075.0	-5619.8	-5625.0	-5840.9	-5962.6
	^4B	-6075.5	-5620.3	-5626.6	-5841.4	-5963.5
	E_{JT}(A)	2.25	1.54	0.61	1.85	1.55
	E_{JT}(B)	2.78	2.07	2.16	2.39	2.48
	$2B$	0.47	0.51	1.55	0.53	0.91
Cu^{2+}						
	^2E(AOC)	-6350.9	--	-5895.3	-6111.8	--
	$^2E(A)$	-6348.7	-5887.0	-5893.9	-6111.4	-6044.1
	$^2E(B)$	-6348.6	-5886.8	-5893.7	-6111.2	-6043.9
	^2A	-6352.8	-5890.8	-5897.8	-6114.6	-6047.8
	^2B	-6353.7	-5891.7	-5898.6	-6115.3	-6048.7
	E_{JT}(A)	4.04	3.80	3.88	3.20	3.70
	E_{JT}(B)	5.12	4.91	4.83	4.06	4.75
	$2B$	0.99	0.95	0.81	0.69	0.89

[a]HS – high-spin; LS – low-spin; IS – intermediate-spin.

[b]Geometry optimizations.

[c]Single point OPBE calculations on LDA geometries.

[d]Single point OPBE calculations with COSMO (water as solvent) on OPBE geometries.

values. From the UV/VIS spectra of $[Cu(TACN)_2]^{2+}$ by Reinen et al.[50] the value of E_{JT} can be estimated as 5.15 kcal·mol^{-1}, while herein we reported 5.12 kcal·mol^{-1} (see Table 3), using the MD-DFT method within LDA approximation. The splitting due to the JT distortion is seen as a band at 7200 cm^{-1} in UV/VIS spectrum, and is reproduced well with TD-DFT (6311 cm^{-1} on LDA geometry and 5893 cm^{-1} on OPBE geometry), as well as with ΔSCF within the LDA approximation (7628 cm^{-1} on LDA geometry). Similarly, E_{JT} for low-spin $[Ni(TACN)_2]^{3+}$ from MD-DFT calculations with LDA functional gives the value of 4.3

kcal·mol^{-1} which is in excellent agreement with the value of 4.6 kcal·mol^{-1} estimated experimentally.[46] It should be pointed out that the JT distortions and E_{JT} in *bis*-TACN complexes are smaller compared to similar N,N-bidentate complexes,[69] because the rigidity of the ligand suppresses significant structural distortion.

The IDP analysis for the $[Cu(TACN)_2]^{2+}$ cation, which gives direct insight what is happening during the distortion is shown in Figure 2. In the C_2 energy minimum conformation $[Cu(TACN)_2]^{2+}$ has 71 totally symmetric normal modes, and all of them are considered in our analysis. A stabilization energy of 5.7 kcal·mol^{-1} in the harmonic approximation used within the IDP model agrees with the MD-DFT calculated one. The skeletal vibrations are coupled with the vibrations of the chelate rings and the normal coordinate analysis is complicated, presenting typical multimode JT problem. Still, we are able to distinguish five skeletal type modes which are the most important for the distortion (they contribute 82% to the total E_{JT}). In Figure 2b, changes of the forces along those five normal modes along the IDP are presented. Analysis of the IDP shows that the distortion starts with the metal–ligand stretching and breathing modes. The contribution of the first one decreases fast along the path, while contribution of metal–ligand stretching however dominates until 60% of the IDP. The importance of skeletal bending increases with increasing deviation from the high symmetry point. All other analyzed systems prone to the JT distortion show the same features, i.e. distortion always start with the hardest modes, while in the second region of the path the softer modes become important and the molecule is simply relaxing towards the global minimum.[55, 69]

Figure 2. IDP analysis for the $[Cu(TACN)_2]^{2+}$ cation

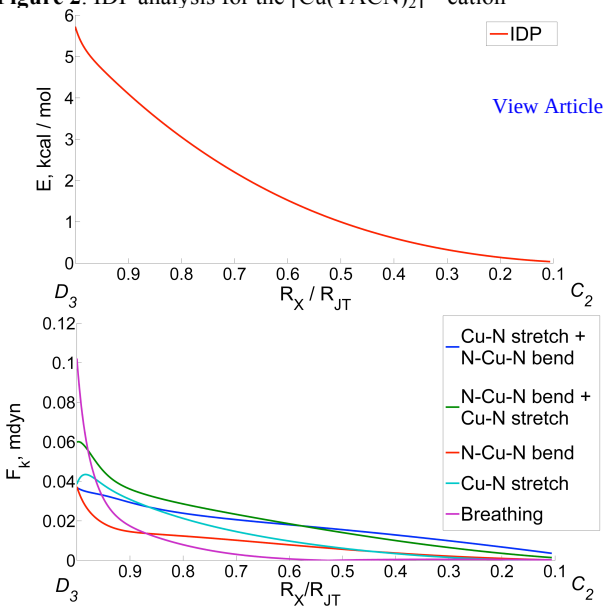

C. UV-Vis spectra of TM complexes

To properly describe UV-VIS spectra, by means of TD-DFT and LF-DFT, we chose the spin state found to be the ground state, in agreement with experimental findings, as shown in Table 1. The energies of the spin-allowed *d-d* excitations, obtained by TD-DFT and LF-DFT, and comparison with experimental transitions for observed ground states are given in Table 4 for the following systems: high-spin $[Cr(TACN)_2]^{3+}$, low-spin $[Fe(TACN)_2]^{3+}$, low-spin $[Co(TACN)_2]^{3+}$, low-spin $[Fe(TACN)_2]^{2+}$, high-spin $[Co(TACN)_2]^{2+}$ and low-spin $[Ni(TACN)_2]^{3+}$.

The Cr^{3+} ion in octahedral environment has a $^4A_{2g}$ ground state and $^4A_{2g}\rightarrow{}^4T_{2g}$ and $^4A_{2g}\rightarrow{}^4T_{1g}$ transitions are observed. Experimentally, band maxima for $[Cr(TACN)_2]^{3+}$ are located around 22750 and 29500 cm^{-1}. LF-DFT nicely reproduces the observed transitions, while for TD-DFT results the comparison with experiment is worse. Cr(III) complexes are known to be problematic for TDDFT, and a total failure to describe the spectrum of CrF_6^{3-} and, to a lesser extent, for $CrCl_6^{3-}$ has already been reported.[85] This is due to the fact that there is a strong Coulomb-repulsion mixing between two excited states.

For the low-spin d^5 $[Fe(TACN)_2]^{3+}$ complex two bands are expected, and both TD-DFT and LF-DFT calculations are consistent and corroborate with experimental spectra, using either the LDA or OPBE geometries.

The UV/VIS spectra for low-spin $[Fe(TACN)_2]^{2+}$ and $[Co(TACN)_2]^{3+}$ show both experimentally and computationally two allowed transitions. TD-DFT results for $[Fe(TACN)_2]^{2+}$ are in good agreement for a second band, but the energy of the first transition is shifted by c.a. 2500-4000 cm^{-1}, depending on the geometry used. LF-DFT results on OPBE geometry reproduce nicely both transitions. The importance of the employed geometries in computations of the excitations can be established from TD-DFT and LF-DFT results for $[Co(TACN)_2]^{3+}$. While the first transition calculated with TD-DFT on LDA geometry is ca. 4000 cm^{-1} higher in energy than experimentally observed, the position of the second transition agrees well. The opposite trend is observed if the OPBE geometry is used. However, LF-DFT results on LDA geometry gives satisfactory agreement with experimentally observed transitions, while the same calculations on OPBE geometry underestimate the position of both bands. It should be pointed out that splitting of the multiplets is better reproduced with LF-DFT method.

The Ni^{3+} complex exhibits the JT distortion of strongly antibonding ^2E state, observed in the ligand field reflection spectra. LF-DFT perfectly matches this band at 6500 cm^{-1}. In addition to the agreement with X-ray structure, this is convincing evidence for the JT distortion. Further bands at 18000 and 24000 cm^{-1} are also reproduced very well with LF-DFT manifold if the OPBE geometry is used. TD-DFT on the same geometry slightly underestimates those transitions.

High-spin $[Co(TACN)_2]^{2+}$ is theoretically predicted to have negligible JT distortion, and it has been found impossible to quantify it experimentally. Thus, the first band in both TD-DFT and LF-DFT is due to the splitting of the degenerate ^4E state. TD-DFT considerably overestimates this splitting, which is in disagreement with the E_{JT} obtained by MD-DFT. The first two transitions (on OPBE geometry) are much better reproduced by LF-DFT than with TD-DFT. Furthermore, the band at 11700 cm^{-1}, typical for the high-spin Co^{2+} compounds is completely missed by TD-DFT, but also shifted by about 4000 cm^{-1} with LF-DFT on LDA geometry. Shoulders at 18348 and 31446 cm^{-1} that appeared in the experimental spectra according to LF-DFT can be tentatively assigned as spin-forbidden transitions.

Table 4 Excitation energies (cm^{-1}) of selected $[M(TACN)_2]^{2+/3+}$ complex ions; $M^{2+/3+}$ is: Cr^{3+}, Fe^{3+}, Co^{3+}, Fe^{2+}, Ni^{3+}, Co^{2+}.

	Assignment			TD-DFT		LF-DFT		
M^{n+}	O_h	D_3	C_2	OPBE-COSMO//LDA[a]	OPBE-COSMO//OPBE[b]	OPBE-COSMO//LDA[a]	OPBE-COSMO//OPBE[b]	Exp.[c]
Cr^{3+}	$^4A_{2g}$	$^4A_2$		0	0	0	0	View Article Online
	$^4T_{2g}$	$^4A_1$		29069	25974	24350	21314	22729
		^4E		29154	26315	24612	22080	
	$^4T_{1g}$	$^4A_2$		30674	27855	28010	25095	29411
		^4E		31055	28169	28638	25715	
Fe^{3+}	$^2T_{2g}$	^2E	^2A	0	0	0	0	
			^2B	4738	5160	1219	1566	
		$^2A_1$	^2A	5581	5721	7229	5944	
	$^2T_{1g}$	$^2A_2$	^2A	18911	16523	21217	19523	20000
		^2E	^2B	19584	16772	21540	19836	
			^2A	20401	17300	22662	21116	
	$^2A_{2g}$	$^2A_2$	^2B	19767	17084	23203	22183	
	^2E_g	^2E	^2A	24605	21999	24300	23234	23255
			^2B	24675	23016	25081	24365	
Co^{3+}	$^1A_{1g}$	$^1A_1$		0	0	0	0	
	$^1T_{1g}$	$^1A_2$		25459	22864	19440	16950	21640
		^1E		25944	23331	19831	17652	
	$^1T_{2g}$	^1E		29585	26954	22175	19941	30030
		$^1A_1$		30395	27820	28198	26175	
Fe^{2+}	$^1A_{1g}$	$^1A_1$		0	0	0	0	
	$^1T_{1g}$	$^1A_2$		21980	19180	20570	18239	16638
		^1E		22796	19963	21203	18259	
	$^1T_{2g}$	$^1A_1$		25447	23186	26296	23463	25839
		^1E		27280	24763	27361	24750	
Ni^{3+}	^2E_g	^2E	^2A	0	0	0	0	
			^2B	5294	5033	6519	6488	6500
	$^2T_{1g}$	^2E	^2A	19716	16927	23276	19962	18000
			^2B	20133	17113	23417	20080	
		$^2A_2$	^2B	22682	19676	26806	23876	
	$^2T_{2g}$	^2E	^2A	22966	19685	27170	24116	24000
			^2B	23470	20665	27484	24325	
		$^2A_1$	^2A	23821	20845	29399	26364	28500
Co^{2+}	$^4T_{1g}$	^4E	^4B	0	0	0	0	
			^4A	5834	6385	60	411	
		$^4A_2$	^4B	6366	6553	231	552	
	$^4T_{2g}$	^4E	^4A	19211	16650	15474	12529	11174
			^4B	20043	17521	15642	12903	
		$^4A_1$	^4A	21065	18797	15764	12999	
	$^4T_{1g}$	$^4A_2$	^4B	22556	20327	16799	14278	15873
		^4E	^4A	26567	25067	17263	15522	
			^4B	26976	25156	17282	15600	
	$^4A_2$	$^4A_2$	^4B	35521	36781	31550	26044	21645

[a]TD-DFT/LF-DFT calculations with OPBE and COSMO on LDA geometries.

[b]TD-DFT/LF-DFT calculations with OPBE and COSMO on OPBE geometries.

[c]Exp. UV/VIS spectra: Cr^{3+}, Fe^{3+}, Fe^{2+}, Co^{2+} ref.[41]; Ni^{3+} ref.[46]; Co^{3+} ref.[38]

Concluding Remarks

We have studied the spin-state preferences of some first-row transition metal ions with TACN ligands, by means of DFT, and determined that both the OPBE and SSB-D functional performed remarkably well for the spin state diversity. Our calculations suggest that the high-spin configuration is favored for $[Cr(TACN)_2]^{3+}$ and $[Mn(TACN)_2]^{2+}$, while the low-spin is computed to be the ground state for $[Fe(TACN)_2]^{3+}$, $[Co(TACN)_2]^{3+}$, $[Fe(TACN)_2]^{2+}$, $[Co(TACN)_2]^{2+}$ and $[Ni(TACN)_2]^{3+}$. Experimentally these predictions have been established for all, but $[Co(TACN)_2]^{2+}$, where the difference between low and high spin states is rather small, and only SSB-D functional was able to capture high-spin as the ground state. Depending on the electronic configuration and occupation of the *d* levels of metal ion, some of the investigated complexes are prone to distortions from D_3 to C_2 due to the vibronic coupling. Even though the JT distortion is sometimes negligible, it must be taken into consideration, because it will lead to itinerant behavior of the unpaired electron/hole which can contribute to all the properties of the system.

TD-DFT with OPBE functional overall reproduces rather well the experimental spectra, but in case of Cr^{3+} and Co^{2+} complexes it clearly failed. This is due to the multideterminantal nature of the transitions, where LF-DFT showed remarkable good results. In LF-DFT both non-dynamical and dynamical correlation are included. The preponderance of evidence suggests that the LF-DFT is particularly good for UV/VIS spectra of transition metal species. All the quantities involved in the calculations are obtained in a non-empirical way, so with this model it is possible not only to interpret the results, but it can also be considered as a reliable tool for the prediction of properties of unknown

coordination compounds.

As final remark one has to notice that treatment of spin states and degenerate states, as well as excited states by means of DFT requires special caution, and their correct description is still challenging for theory. However, the good ability of both OPBE and SSB-D functionals to predict spin states, as well as good perfomance of MD-DFT for treatment of degenerate and excited states, as demonstrated in this work, are encouraging.

Acknowledgments

The following organizations are thanked for financial support: the HPC-Europa2 Transnational Access program of the European Union, the Ministerio de Ciencia e Innovación (MICINN, project number CTQ2011-25086/BQU), and the DIUE of the Generalitat de Catalunya (project number 2009SGR528), and Serbian Ministry of Science under project 172035. Financial support from MICINN (Ministry of Science and Innovation, Spain) and the FEDER fund (European Fund for Regional Development) was provided by grant UNGI08-4E-003.

Notes and references

[a] *Center for Chemistry, IHTM, University of Belgrade, Studentski trg 12–16, 11000 Belgrade, Serbia*
[b] *Faculty of Chemistry, University of Belgrade, Studentski trg 12–16, 11000 Belgrade, Serbia; E-mail: gmaja@chem.bg.ac.rs*
[c] *Institut de Química Computacional and Departament de Química, Universitat de Girona, Campus Montilivi, Facultat de Ciències, 17071 Girona, Spain*
[d] *Institució Catalana de Recerca i Estudis Avançats (ICREA), Pg. Lluís Companys 23, 08010 Barcelona, Spain. Fax: +34 972 418356; Tel: +34 972 418861; E-mail: marcel.swart@icrea.cat*

† Electronic Supplementary Information (ESI) available: coordinates of all species, and bond lengths. See DOI: 10.1039/b000000x/†

‡ Footnotes should appear here. These might include comments relevant to but not central to the matter under discussion, limited experimental and spectral data, and crystallographic data.

1. J. N. Harvey, R. Poli and K. M. Smith, *Coord. Chem. Rev.*, 2003, **238-239**, 347-361.
2. J. N. Harvey, *Struct. Bond.*, 2004, **112**, 151-183.
3. M. Swart, *Int. J. Quantum Chem.*, 2012, doi: 10.1002/qua.24255.
4. M. Swart, M. Guell and M. Sola, in *Quantum Biochemistry: Electronic Structure and Biological Activity*, ed. C. F. Matta, Wiley-VCH: Weinheim-Germany, 2010, pp. 551-583.
5. P. Gütlich, A. Hauser and H. Spiering, *Angew. Chem. Int. Ed.*, 1994, **33**, 2024-2054.
6. H. Paulsen, L. Duelund, H. Winkler, H. Toftlund and A. X. Trautwein, *Inorg.Chem.*, 2001, **40**, 2201-2203.
7. P. Gütlich and H. A. Goodwin, in *Spin Crossover in Transition Metal Compounds I*, eds. P. Gütlich and H. A. Goodwin, Springer Berlin / Heidelberg, 2004, vol. 233, pp. 1-47.
8. M. P. Shaver, L. E. N. Allan, H. S. Rzepa and V. C. Gibson, *Angew. Chem. Int. Ed.*, 2006, **45**, 1241-1244.
9. J.-F. Létard, P. Guionneau and L. Goux-Capes, in *Spin Crossover in Transition Metal Compounds III*, eds. P. Gütlich and H. A. Goodwin, Springer Berlin / Heidelberg, 2004, vol. 235, pp. 1-19.
10. H. A. Jahn and E. Teller, *Proc. R. Soc. London, Ser. A*, 1937, **161**, 220-235.
11. I. B. Bersuker, *The Jahn-Teller Effect*, Cambridge University Press, 2006.
12. R. G. Parr and W. Yang, *Density-Functional Theory of Atoms and Molecules*, Oxford University Press, 1989.
13. R. M. Dreizler and E. K. U. Gross, *Density Functinal Theory, An Approach to Quantum Many-Body Problem*, Springer-Verlag Berlin, Heidelberg, New York, London, Paris, Tokyo, Hong Kong, Barcelona, 1990.
14. W. Koch and M. C. Holthausen, *A Chemist's Guide to Density Functional Theory*, Wiley-VCH, Weinhem, 2000.
15. M. Swart, A. R. Groenhof, A. W. Ehlers and K. Lammertsma, *J. Phys. Chem. A*, 2004, **108**, 5479-5483.
16. C. R. Jacob and M. Reiher, *Int. J. Quantum Chem.*, 2012, doi: 10.1002/qua.24309.
17. M. Güell, J. M. Luis, M. Solà and M. Swart, *J. Phys. Chem. A*, 2008, **112**, 6384-6391.
18. J. Conradie and A. Ghosh, *J. Phys. Chem. B*, 2007, **111**, 12621-12624.
19. M. Swart, *J. Chem. Theory Comput.*, 2008, **4**, 2057–2066.
20. M. Swart, A. W. Ehlers and K. Lammertsma, *Mol. Phys.*, 2004, **102**, 2467-2474.
21. N. C. Handy and A. J. Cohen, *Mol. Phys.*, 2001, **99**, 403-412.
22. J. P. Perdew, K. Burke and M. Ernzerhof, *Phys. Rev. Lett.*, 1996, **77**, 3865-3868
23. M. Güell, M. Solà and M. Swart, *Polyhedron*, 2010, **29**, 84-93.
24. J. Conradie and A. Ghosh, *J. Chem. Theory Comput.*, 2007, **3**, 689-702.
25. E. Derat, D. Kumar, R. Neumann and S. Shaik, *Inorg. Chem.*, 2006, **45**, 8655-8663.
26. A. R. Groenhof, A. W. Ehlers and K. Lammertsma, *J. Am. Chem. Soc.*, 2007, **129**, 6204-6209.
27. M.-S. Liao, J. D. Watts and M.-J. Huang, *J. Comput. Chem.*, 2006, **27**, 1577-1592.
28. M.-S. Liao, J. D. Watts and M.-J. Huang, *J. Phys. Chem. A*, 2007, **111**, 5927-5935.
29. S. Romo, J. A. Fernández, J. M. Maestre, B. Keita, L. Nadjo, C. de Graaf and J. M. Poblet, *Inorg. Chem.*, 2007, **46**, 4022-4027.
30. C. Rong, S. Lian, D. Yin, B. Shen, A. Zhong, L. Bartolotti and S. Liu, *J. Chem. Phys.*, 2006, **125**, 174102.
31. M. Swart, *Inorg. Chim. Acta*, 2007, **360**, 179-189.
32. I. Wasbotten and A. Ghosh, *Inorg. Chem.*, 2006, **45**, 4910-4913.
33. A. Wu, Y. Zhang, X. Xu and Y. Yan, *J. Comput. Chem.*, 2007, **28**, 2431-2442.
34. S. Zein, S. A. Borshch, P. Fleurat-Lessard, M. E. Casida and H. Chermette, *J. Chem. Phys.*, 2007, **126**, 014105.
35. M. Swart, M. Solà and F. M. Bickelhaupt, *J. Chem. Phys.*, 2009, **131**, 094103.
36. M. Swart, M. Solà and F. M. Bickelhaupt, *J. Comput. Methods Sci. Eng.*, 2009, **9**, 69-77.
37. P. Chaudhuri and K. Wieghardt, in *Progress in Inorganic Chemistry*, ed. S. J. Lippard, John Wiley & Sons, Inc., New York, 1987, pp. 329-436.
38. H. Koyama and T. Yoshino, *Bull. Chem. Soc. Jpn.*, 1972, **45**, 481-484.
39. R. Yang and L. J. Zompa, *Inorg. Chem.*, 1976, **15**, 1499-1502.
40. L. J. Zompa, *Inorg. Chem.*, 1978, **17**, 2531-2536.
41. K. Wieghardt, W. Schmidt, W. Herrmann and H. J. Kuppers, *Inorg. Chem.*, 1983, **22**, 2953-2956.
42. A. Kromm and W. S. Sheldrick, *Acta Crystallogr. Sect. E: Struct. Rep. Online*, 2007, **63**, M581-M583.
43. J. C. A. Boeyens, A. G. S. Forbes, R. D. Hancock and K. Wieghardt, *Inorg. Chem.*, 1985, **24**, 2926-2931.
44. H. J. Kuppers, A. Neves, C. Pomp, D. Ventur, K. Wieghardt, B. Nuber and J. Weiss, *Inorg. Chem.*, 1986, **25**, 2400-2408.
45. L. J. Zompa and T. N. Margulis, *Inorg. Chim. Acta*, 1978, **28**, L157-L159.
46. K. Wieghardt, W. Walz, B. Nuber, J. Weiss, A. Ozarowski, H. Stratemeier and D. Reinen, *Inorg. Chem.*, 1986, **25**, 1650-1654.
47. P. Chaudhuri, C. Stockheim, K. Wieghardt, W. Deck, R. Gregorzik, H. Vahrenkamp, B. Nuber and J. Weiss, *Inorg. Chem.*, 1992, **31**, 1451-1457.
48. R. L. Lord, F. A. Schultz and M. H. Baik, *J. Am. Chem. Soc.* , 2009, **131**, 6189-6197.
49. F. A. Schultz, *J. Solid. State. Electrochem.*, 2011, **15**, 1833-1843.
50. P. Chaudhuri, K. Oder, K. Wieghardt, J. Weiss, J. Reedijk, W. Hinrichs, J. Wood, A. Ozarowski, H. Stratemaier and D. Reinen, *Inorganic Chemistry*, 1986, **25**, 2951-2958.

51. M. Kavana, D. R. Powell and J. N. Burstyn, *Inorganica Chimica Acta*, 2000, **297**, 351-361.
52. R. Bruyndonckx, C. Daul, P. T. Manoharan and E. Deiss, *Inorg. Chem.*, 1997, **36**, 4251-4256.
53. M. Zlatar, C.-W. Schlaepfer and C. Daul, in *The Jahn-Teller-Effect Fundamentals and Implications for Physics and Chemistry*, eds. H. Koeppel, D. R. Yarkoni and H. Barentzen, Springer, Heidelberg, Dordrecht, London, New York, 2009, vol. 97, pp. 131-165.
54. M. Zlatar, M. Gruden-Pavlovic, C.-W. Schlaepfer and C. Daul, *J. Mol. Struc. THEOCHEM*, 2010, **954**, 86-93.
55. M. Gruden-Pavlović, P. Garcia-Fernandez, L. Andjelković, C. Daul and M. Zlatar, *J. Phys.Chem. A*, 2011, **115**, 10801-10813.
56. E. J. Baerends, J. Autschbach, A. Bérces, J. A. Berger, F. M. Bickelhaupt, C. Bo, P. L. de Boeij, P. M. Boerrigter, L. Cavallo, D. P. Chong, L. Deng, R. M. Dickson, D. E. Ellis, M. van Faassen, L. Fan, T. H. Fischer, C. Fonseca Guerra, S. J. A. van Gisbergen, J. A. Groeneveld, O. V. Gritsenko, M. Grüning, F. E. Harris, P. van den Hoek, C. R. Jacob, H. Jacobsen, L. Jensen, E. S. Kadantsev, G. van Kessel, R. Klooster, F. Kootstra, E. van Lenthe, D. A. McCormack, A. Michalak, J. Neugebauer, V. P. Nicu, V. P. Osinga, S. Patchkovskii, P. H. T. Philipsen, D. Post, C. C. Pye, W. Ravenek, P. Romaniello, P. Ros, P. R. T. Schipper, G. Schreckenbach, J. G. Snijders, M. Solà, M. Swart, D. Swerhone, G. te Velde, P. Vernooijs, L. Versluis, L. Visscher, O. Visser, F. Wang, T. A. Wesolowski, E. M. van Wezenbeek, G. Wiesenekker, S. K. Wolff, T. K. Woo, A. L. Yakovlev and T. Ziegler, *ADF 2012.01*, (2012) SCM, Amsterdam.
57. G. te Velde, F. M. Bickelhaupt, S. J. A. van Gisbergen, C. F. Guerra, E. J. Baerends, J. G. Snijders and T. Ziegler, *J. Comput. Chem.*, 2001, **22**, 931-967.
58. C. F. Guerra, J. G. Snijders, G. te Velde and E. J. Baerends, *Theor. Chem. Acc.*, 1998, **99**, 391-403.
59. E. van Lenthe and E. J. Baerends, *J. Comput. Chem.*, 2003, **24**, 1142-1156.
60. S. H. Vosko, L. Wilk and M. Nusair, *Can. J. Phys.*, 1980, **58**, 1200-1211.
61. M. Swart and F. M. Bickelhaupt, *J. Comput. Chem.*, 2008, **29**, 724-734.
62. M. Swart and F. M. Bickelhaupt, *Int. J. Quantum Chem.*, 2006, **106**, 2536-2544.
63. A. Klamt and G. Schüürmann, *J. Chem. Soc.,Perkin Trans. 2*, 1993, 799-805.
64. A. Klamt, *J. Phys. Chem.*, 1995, **99**, 2224-2235.
65. A. Klamt and V. Jones, *J. Chem. Phys.*, 1996, **105**, 9972-9981.
66. C. C. Pye and T. Ziegler, *Theor. Chem. Acc.*, 1999, **101**, 396-408.
67. M. Swart, E. Rösler and F. M. Bickelhaupt, *Eur. J. Inorg. Chem.*, 2007, **2007**, 3646-3654.
68. L. Andjelković, M. Gruden-Pavlović, C. Daul and M. Zlatar, *Int. J. Quantum Chem.*, 2012, doi: 10.1002/qua.24245.
69. M. Gruden-Pavlović, M. Zlatar, C.-W. Schlaepfer and C. Daul, *J. Mol. Struc. THEOCHEM*, 2010, **954**, 80-85.
70. T. K. Kundu, R. Bruyndonckx, C. Daul and P. T. Manoharan, *Inorg. Chem.*, 1999, **38**, 3931-3934.
71. E. K. U. Gross, J. F. Dobson and M. Petersilka, in *Density Functional Theory II*, ed. R. F. Nalewajski, Springer, Heidelberg, 1996, vol. 181, pp. 81-172.
72. S. J. A. van Gisbergen, J. G. Snijders and B. E.J., *Comput. Phys. Commun.*, 1999, **118**, 119-138.
73. M. A. Atanasov, C. A. Daul and C. Rauzy, *Chem. Phys. Lett.*, 2003, **367**, 737-746.
74. M. A. Atanasov, C. A. Daul and C. Rauzy, *Struct. Bond.*, 2004, **106**, 97-125.
75. M. A. Atanasov, C. Rauzy, P. Baettig and C. A. Daul, *Int. J. Quantum Chem.*, 2005, **102**, 119-131.
76. M. A. Atanasov, E. J. Baerends, P. Baettig, R. Bruyndonckx, C. Daul, C. Rauzy and M. Zbiri, *Chem. Phys. Lett.* , 2004, **399**, 433-439.
77. M. A. Atanasov and C. A. Daul, *Comptes. Rendus. Chimie*, 2005, **8**, 1421-1433.
78. M. A. Atanasov and C. A. Daul, *Chimia* 2005, **59**, 504-510.
79. M. Atanasov, C. Daul, M. Rohmer and T. Venkatachalam, *Chem. Phys. Lett.*, 2006, **427**, 449-454.
80. K. Pierloot and S. Vancoillie, *J. Chem. Phys.*, 2006, **125**, 124303-124309.
81. M. R. Bray, R. J. Deeth, V. J. Paget and P. D. Sheen, *Int. J. Quantum Chem.*, 1996, **61**, 85-91.
82. A. R. Groenhof, M. Swart, A. W. Ehlers and K. Lammertsma, *J. Phys. Chem. A*, 2005, **109**, 3411-3417.
83. M. Swart, M. Güell, J. M. Luis and M. Solà, *J. Phys. Chem. A*, 2010, **114**, 7191-7197.
84. J. W. Turner and F. A. Schultz, *Inorg. Chem.*, 2001, **40**, 5296-5298.
85. M. Atanasov, P. Comba, C. A. Daul and F. Neese, in *Models, Mysteries and Magic of Molecules*, eds. J. C. A. Boeyens and J. F. Ogilvie, Springer, Dordrecht, The Netherlands, 2008, pp. 411-445.